

[Electronic Supplementary Information]

Metal-Enhanced Fluorescence of Dyes with Quadrupole Surface Plasmon Resonance of Silver Nanoparticles

Daedu Lee, Junghyun Song, Gyoungyun Song, and Yoonsoo Pang*

Department of Chemistry, Gwangju Institute of Science and Technology, 123

Cheomdangwagi-ro, Buk-gu, Gwangju 61005, Republic of Korea

*Author to whom correspondence should be addressed. E-mail address: ypang@gist.ac.kr

Table of Contents

1. Extinction spectra of silver colloidal nanoparticles in water.....	2
2. Measurement for the thickness of polystyrene films	3
3. Mesh convergence test for the electric field simulations by FDTD method.....	5
4. Charge density distributions for the dipole and quadrupole surface plasmon resonances of silver nanoparticles	7
5. Emission kinetics of DCM, DNBP, and C343 with the SCFs	9

1. Extinction spectra of silver colloidal nanoparticles in water

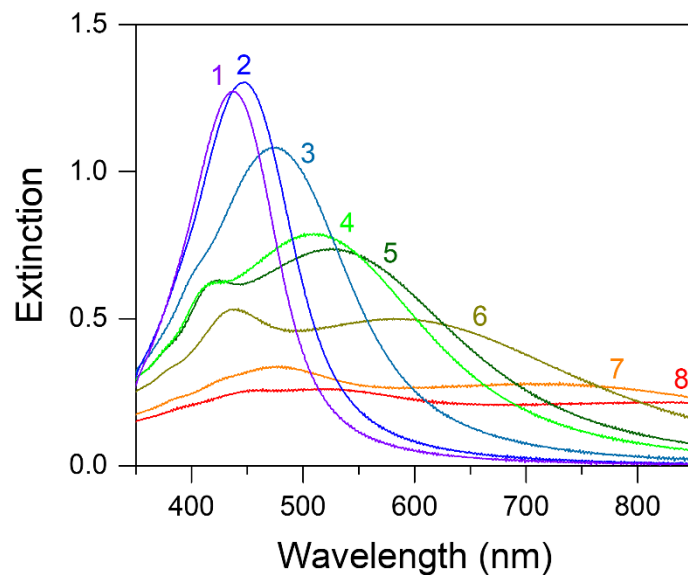


Figure S1. (a) Steady-state extinction spectra of silver colloidal nanoparticles dispersed in water, which were labeled as 1-8 (SCF1-SCF8) with the increase of average particle diameter from 59 to 219 nm. The dipole SPR bands only appear in the spectra of the small silver nanoparticles (1-3; 59-93 nm in diameter), and the quadrupole SPR bands appear in the spectra of the larger silver nanoparticles (4-8; 116-219 nm in diameter), in shorter wavelengths than those of the dipole bands.

2. Measurement for the thickness of polystyrene films

The thickness of the PS films prepared by spin-coating with the 1% (w/v) polystyrene (PS) solution was estimated by the interference patterns present in the UV-VIS absorption spectra.^{42,}

⁴³ The thickness of the PS films, d was evaluated by eq. 1,

$$d = \frac{N_{cyc} \lambda_1 \lambda_2}{2(n_1 \lambda_2 + n_2 \lambda_1)} \quad (1)$$

where N_{cyc} is the number of cycles between wavelength λ_1 and λ_2 observed in UV-VIS spectrum (Fig. S2(a)), and n_1 and n_2 the refractive indices of the PS medium at the λ_1 and λ_2 , respectively.

The refractive indices of the PS medium were evaluated as follows.¹

$$n_\lambda = 0.4368 - 1.052 \times \lambda \text{ (in nm)} \quad (2)$$

As shown in Fig. S2(b), the thickness of the PS films strongly depends on the concentration of the THF solution. The thickness of the PS films spin-coated with the 4% solution was 620 nm and the thickness of 180 nm was determined for the PS films prepared with the 1% PS solution in THF. Thus, the thickness of the PS films used in the fluorescence enhancement study with the SCFs was determined as thin as 180 nm.

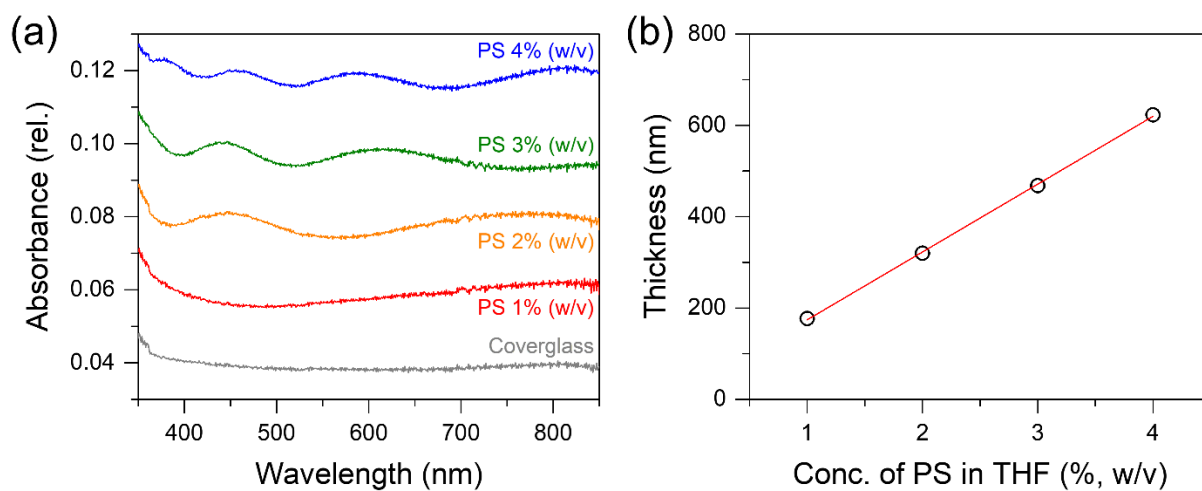


Figure S2. (a) Absorption spectra of the PS films spin-coated with the 1-4% (w/v) PS solutions in THF; (b) the thickness of the PS films shows a strong dependence on the concentration of the PS solution.

3. Mesh convergence test for the electric field simulations by FDTD method

We performed the mesh convergence test for the electric field distribution simulations for the silver nanoparticles with 59 nm (SCF1) and 129 nm (SCF5) in diameter by FDTD. As shown in Fig. S3, the averaged values for the square of the electric field strength in the range of 0-50 nm from the nanoparticle's surface only showed minor dependence on the mesh size. Compared the results with the smallest mesh size adopted (2.24 with 0.5 nm mesh) for the SCF1, the square values of electric field increase with the increase of the mesh size by 0.4-1.8% (2.25 with 0.75 nm and 2.28 with 1.0 nm mesh). The dependence on the mesh size becomes further decreased in the simulations for the larger nanoparticles. The increase of the mesh size from 0.5 nm to 0.75 and 1.0 nm in the simulations for the SCF5 induces only small increases in the square values of the electric field as 2.01 \rightarrow 2.02 (increased by 0.5%) and 2.04 (increased by 1.5%), respectively. With these results, we concluded that the mesh size of 1.0 nm for all the FDTD simulations used in this work is justified. The simulations with the smaller mesh size requires longer simulation time proportional to $1/(\text{mesh size})^2$ with small changes in the calculated values of the square of the electric field around each silver nanoparticle.

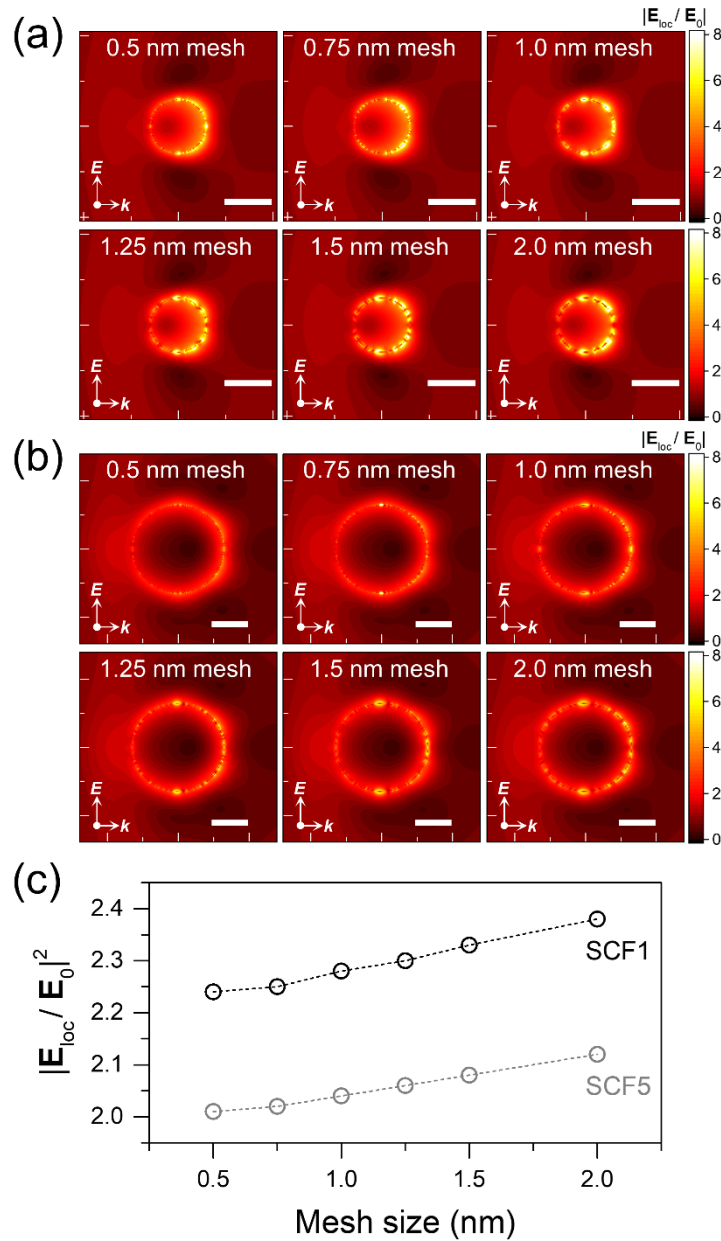


Figure S3. (a) Local electric field distributions around the silver nanoparticles of (a) 59 nm (SCF1) and (b) 129 nm (SCF5) in diameter calculated by the FDTD simulations with the mesh sizes of 0.5-2.0 nm, (c) $|E_{loc}/E_0|^2$ values averaged within 50 nm from the surface of silver nanoparticles of 59 nm (SCF1) and 129 nm (SCF5) as a function of the mesh size. All the scale bars in panels (a) and (b) are 50 nm long.

4. Charge density distributions for the dipole and quadrupole surface plasmon resonances of silver nanoparticles

The surface charge density distributions at the maximum wavelengths for the dipole and quadrupole SPR bands of the SCF5 (446 and 657 nm, respectively) and SCF8 (523 and 900 nm) were obtained by the FDTD simulations. The surface charge density distributions obtained in the plane including the electric field and wave vector of the incident electromagnetic radiation, for the silver nanoparticles of the SCF5 and SCF8 were shown in Fig. S4. The charge distributions obtained at 657 nm for SCF5 and 900 nm for SCF8 represent the dipole SPR with the nodal plane perpendicular to the electric field vector of the incident radiation. On the other hand, the charge distributions obtained with at 446 nm for SCF5 and 523 nm for SCF8 represent the quadrupole SPR with two nodal planes perpendicular to the electric field vector or the wave vector of the incident radiation. With these simulation results, the assignments for the dipole and quadrupole SPR bands of the SCF1-SCF8 can be justified.

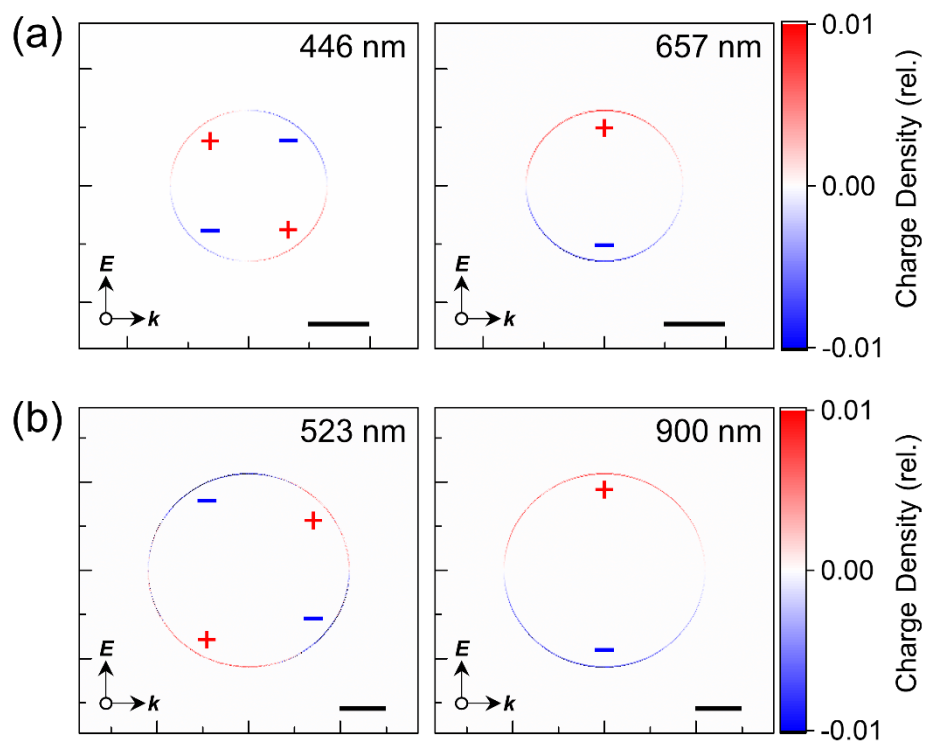


Figure S4. Charge density distributions of the silver nanoparticles with (a) 129 nm in diameter (SCF5) at 446 and 657 nm and (b) 219 nm in diameter (SCF8) at 523 and 900 nm calculated by the FDTD simulation. All the scale bars are 50 nm long.

5. Emission kinetics of DCM, DNBP, and C343 with the SCFs

The fluorescence kinetics of DCM, DNBP, and C343 with and without SCFs shown in Fig. 4 were fit with the exponential functions convoluted with the Gaussian instrument response function,

$$GE_i(t) = A_i \exp\left(\frac{\omega^2}{2\tau_i^2} - \frac{t-t_0}{\tau_i}\right) \left[1 - \operatorname{erf}\left(\frac{\omega^2 - \tau_i(t-t_0)}{\sqrt{2}\omega\tau_i}\right)\right] \quad (\text{S2})$$

where A_i denotes the amplitude, τ_i the exponential lifetime, and ω the bandwidth of a Gaussian function. The emission kinetics and the intensity average lifetimes of the dyes with and without the SCFs are summarized in Table S1, and the fit results of DNBP with and without the SCFs were shown in Fig. S5 as an example.

Table S1. Emission kinetics of DCM, DNBP, and C343 with the SCFs ^a

SCF	a_1	τ_1 (ns)	a_2	τ_2 (ns)	$\bar{\tau}$ (ns) ^b
DCM					
w/o SCF	0.517	0.42	0.483	1.76	1.49
SCF1	0.691	0.24	0.309	1.30	0.99
SCF2	0.724	0.21	0.276	1.19	0.88
SCF3	0.654	0.25	0.346	1.31	1.03
SCF4	0.593	0.28	0.407	1.45	1.19
SCF5	0.550	0.30	0.450	1.50	1.26
SCF6	0.598	0.26	0.402	1.45	1.20
SCF7	0.652	0.28	0.348	1.34	1.04
SCF8	0.684	0.26	0.316	1.23	0.93
DNBP					
w/o SCF	0.377	0.50	0.623	2.33	2.12
SCF1	0.708	0.19	0.292	1.52	1.21
SCF2	0.700	0.20	0.300	1.54	1.23
SCF3	0.644	0.22	0.356	1.68	1.40
SCF4	0.470	0.35	0.530	2.10	1.88
SCF5	0.510	0.30	0.490	1.96	1.73
SCF6	0.561	0.26	0.439	1.88	1.64
SCF7	0.645	0.24	0.355	1.62	1.33
SCF8	0.615	0.26	0.385	1.69	1.41
C343					
w/o SCF	–	–	1.000	2.54	–
SCF1	0.373	0.41	0.627	1.99	1.82
SCF2	0.299	0.46	0.701	2.20	2.05
SCF3	0.250	0.65	0.750	2.49	2.34
SCF4	0.240	0.82	0.760	2.63	2.47
SCF5	0.298	0.53	0.702	2.36	2.20
SCF6	0.345	0.46	0.655	2.14	1.97
SCF7	0.341	0.46	0.659	2.37	2.19
SCF8	0.286	0.59	0.714	2.43	2.27

^a The emission kinetics of DCM, DNBP, and C343 were probed at 555, 505, and 465 nm, respectively.

^b The intensity average lifetime, $\bar{\tau} = \frac{a_1\tau_1^2 + a_2\tau_2^2}{a_1\tau_1 + a_2\tau_2}$.⁵⁶

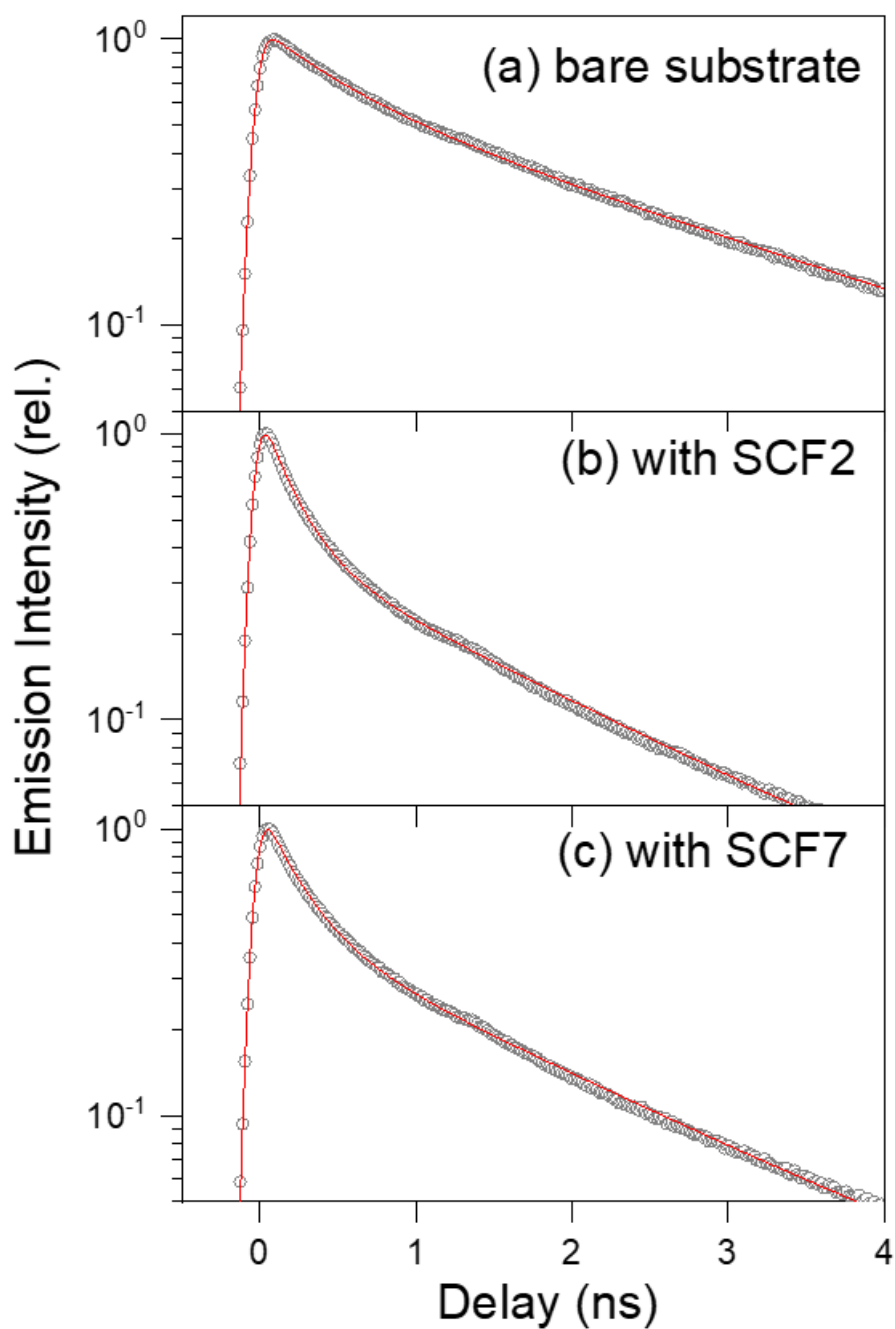


Figure S5. Fluorescence kinetics and experimental fit results of DNBP probed at 505 nm with (a) bare substrate, (b) SCF2, and (c) SCF7. The hollow circles represent the experimental data and the red lines represent the exponential fit results convoluted with the Gaussian instrument response function.

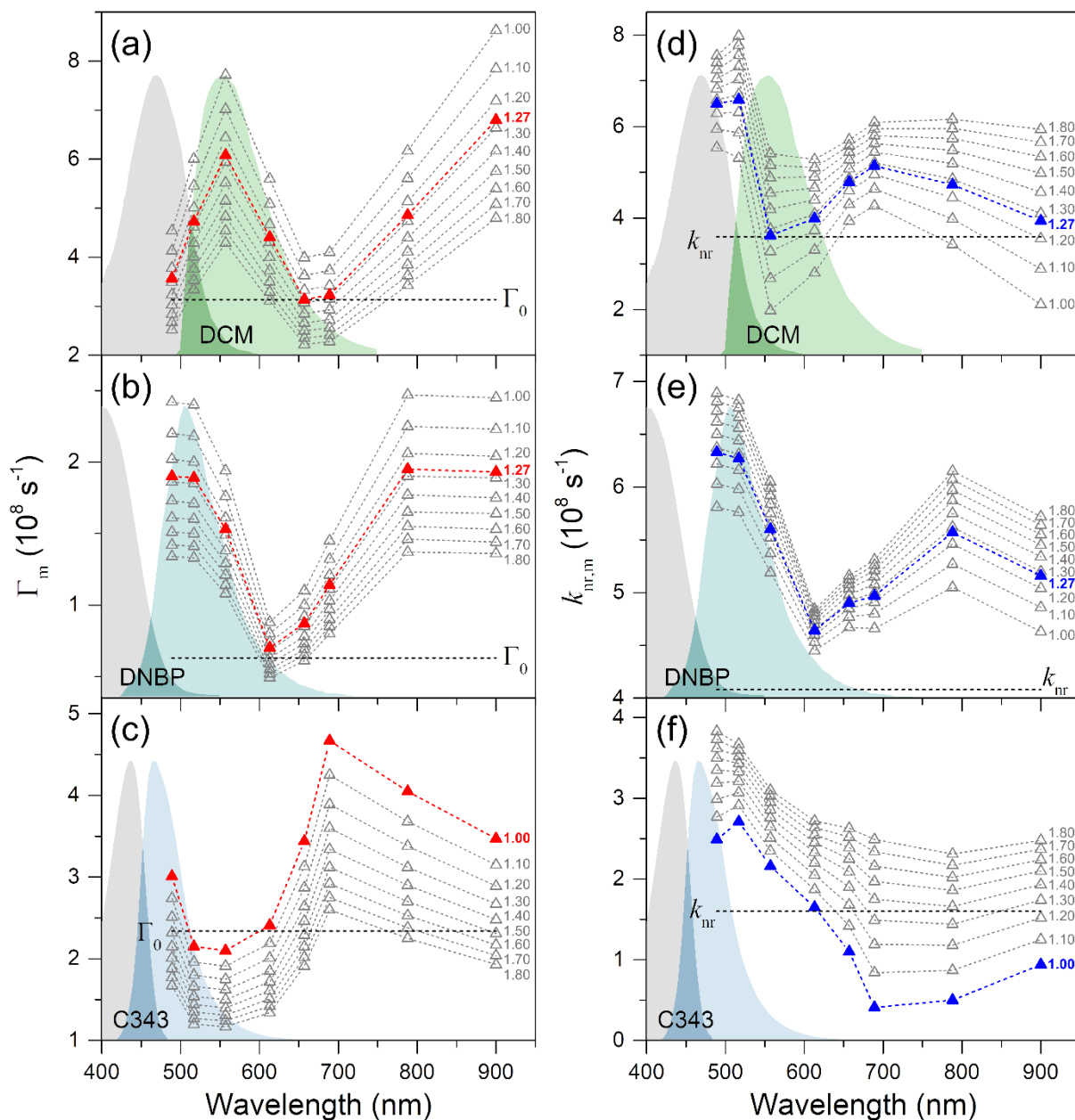


Figure S6. Radiative constants (Γ_m) of (a) DCM, (b) DNBP, and (c) C343, and the non-radiative rate constants ($k_{nr,m}$) of (d) DCM, (e) DNBP, and (f) C343 with the SCFs estimated by the improved semi-empirical model with the proportionality coefficient range of $\gamma = 1.00$ -1.80. The $\gamma = 1.27$ was used for the Γ_m and $k_{nr,m}$ of DCM and DNBP, and $\gamma = 1.00$ was used for C343. The radiative (Γ_0) and non-radiative rate constants (k_{nr}) of each dye obtained without the SCFs were also displayed as black dashed lines for comparison.

References

1. N. Sultanova, S. Kasarova and I. Nikolov, *Acta Phys. Pol., A*, 2009, **116**, 585-587.